Applying XAS to Your Research: Theory Overview and Application to YBCO

Trevor A. Tyson

Department of Physics

New Jersey Institute of Technology

Transition metal oxide systems display a broad range of interesting and intriguing properties such as light induced changes in resistivity, superconductivity and high magnetoresistance. Materials of this class can be driven from an insulating to a metallic state by the applications of pressure, magnetic or electric fields. The properties of these materials depend on a delicate balance of long range and short range forces. Consequently, the behavior of these materials is strongly influenced by local no-periodic structural distortions. Synchrotron based x-ray absorption measurements provide unique insight into the structure-transport correlations. In this talk, simultaneous photododoping and x-ray absorption experiments on YBCO will be presented and the photo-induced charge transfer and structural changes will be discussed. An outline of the theoretical framework will also be given.

I. X-Ray Absorption Spectroscopy (XAS)-Theory Overview

See:

J. J.Rehr and R. C. Albers, Rev. Mod. Phys. **72**, 621 (200) and references therein.

T. A. Tyson, K. O. Hodgson, C. R. Natoli and M. Benfatto, Phys. Rev. B 46, 5997 (1992) and references therein.

Recall expression for cross section

$$\sigma(\hbar\omega) = 4\pi^2 \alpha \hbar\omega \sum_{if} |\langle\psi_f|\hat{\varepsilon}\cdot\vec{r}\,|\psi^i_{core}\rangle|^2 \delta(\hbar\omega + E_i - E_f)$$

$$= 4\pi^2 \alpha \hbar\omega \sum_{if} \langle\psi^i_{core}|\hat{\varepsilon}\cdot\vec{r}\,\delta(\hbar\omega + E_i - E_f)\,|\psi_f\rangle$$

$$\langle\psi_f|\hat{\varepsilon}\cdot\vec{r}\,|\psi^i_{core}\rangle$$

This can be written in terms of the Green's function of the cluster by using the identity

$$\lim_{\eta\to 0^+} \frac{1}{x \pm i\eta} = P\,\frac{1}{x} \mp i\pi\delta(x)$$

$$\delta(\hbar\omega + E_i - E_f)\,|\psi_f\rangle = \delta(\hbar\omega + E_i - H_o)\,|\psi_f\rangle$$

$$= \frac{-1}{\pi} \lim_{\eta\to 0^+} \mathrm{Im}\left[\frac{1}{\hbar\omega + E_i - H_o + i\eta}\right] |\psi_f\rangle$$

$$= \mathrm{Im}\left[\frac{-1}{\pi} G^+(E)\right] |\psi_f\rangle$$

$E = \hbar\omega + E_i$

Hence we obtain the cross section

$$\sigma(\hbar\omega) = 4\pi^2 \alpha \hbar\omega \sum_i \mathrm{Im}\left[\langle \psi^i_{core} | \hat{\varepsilon}\cdot\vec{r} \left[\frac{-1}{\pi} G^+(\vec{r},\vec{r}';E) \right] \hat{\varepsilon}\cdot\vec{r}' | \psi^i_{core} \rangle \right]$$

$$= 4\pi^2 \alpha \hbar\omega \sum_i \mathrm{Im}\{ \iint d^3r\, d^3r'\, \psi^i_{core}(\vec{r})\, \hat{\varepsilon}\cdot\vec{r} \left[\frac{-1}{\pi} G(\vec{r},\vec{r}',E) \right] \hat{\varepsilon}\cdot\vec{r}'\, \psi^i_{core}(\vec{r}') \}$$

where the Green's function satisfies

$$H_0\, G^+(\vec{r},\vec{r}',E) = [\nabla^2 + E - V(\vec{r})]\, G^+(\vec{r},\vec{r}',E) = \delta(\vec{r}-\vec{r}')$$

For the case of a muffin-tin type of potential (no overlaps) the Green's function is found to be

$$\frac{-1}{\pi}\left[G^+(\vec{r},\vec{r}',E)\right]^{ij}_{LL'} = \sum_{LL'} R^i_L(\vec{r})\, \tau^{ij}_{LL'}\, R^j_{L'}(\vec{r}') - \sum_L \delta_{ij}\, R^i_L(\vec{r}_<)\, S^i_L(\vec{r}_>)$$

but for the case of inner-shell excitations we need only the form

$$\frac{-1}{\pi}\left[G^+(\vec{r},\vec{r}',E)\right] = \sum_{LL'} R^0_L(\vec{r})\, \tau^{00}_{LL'}\, R^0_{L'}(\vec{r}') - \sum_L R^0_L(\vec{r}_<)\, S^0_L(\vec{r}_>)$$

where $\vec{r}$ and $\vec{r}'$ are centered on the absorber's sphere and we define

$$\vec{r}_< \equiv \begin{cases} \vec{r} & \text{for } r < r' \\ \vec{r}' & \text{for } r' < r \end{cases}$$

and similarly

$$\vec{r}_{>} \equiv \begin{cases} \vec{r} & \text{for } r > r' \\ \vec{r'} & \text{for } r' > r \end{cases}.$$

The final state wave function

$$R^{0}_{L}(\vec{r}) = R^{0}_{l}(\vec{r})\, Y_{L}(\hat{r})$$

has the radial part $R^{0}_{l}(\vec{r})$ that is the regular solution of the radial Schrödinger equation inside the absorber's sphere and matches on to (K-matrix normalization)

$$\sqrt{\frac{\kappa}{\pi}}[j_{l}(\kappa r)\cot(\delta_{l}) - n_{l}(\kappa r)]$$

with

$$\kappa \equiv \sqrt{E - V_{II}}$$

at the sphere radius. The solution

$$S^{0}_{L}(\vec{r}) = S^{0}_{l}(\vec{r})\, Y_{L}(\hat{r})$$

is the singular (unbounded at the sphere origin) one and matches

$$\sqrt{\frac{\kappa}{\pi}} j_{l}(\kappa r).$$

$$\tau = T_a + T_a G_0 T_a + T_a G_0 T_a G_0 T_a + T_a G_0 T_a G_0 T_a G_0 T_a + \cdots$$

$$\tau = T_a + T_a G_0 \tau \cdot$$

or

$$\tau = [1 - T_a G_0]^{-1} T_a \cdot$$

In angular momentum representation we write down the site diagonal T-matrix and free Green's function as

$$(T_a^{-1})^{ij}_{L\,L'} = [(t^i_l)^{-1}]\, \delta_{ij}\, \delta_{L\,L'}$$

$$(t^i_l)^{-1} = \frac{W[-ih^+_l, R^i_l]}{W[j_l, R^i_l]} = \frac{W[n_l, R^i_l]}{W[j_l, R^i_l]} - i = \cot(\delta^i_l) - i = \left[\sin(\delta^i_l)\, e^{i\delta^i_l}\right]^{-1}$$

$$W[f,g] = fg' - f'g$$

$$G^{ij}_{LL'} = -4\pi i\,(1 - \delta_{ij}) \sum_{L''} i^{l-l'+l''} C^{L'}_{LL''} h^+_{l''}(\kappa R_{ij}) Y_{L''}(\hat{R}_{ij})$$

$$C^{L'}_{LL''} = \int d\Omega Y_L(\Omega) Y^*_{L'}(\Omega) Y_{L''}(\Omega)$$

and

$$\vec{R}_{ij} = \vec{R}_i - \vec{R}_j.$$

The unpolarized cross section is then

$$\sigma(\hbar\omega) = \frac{8}{3}\pi^2 \alpha \hbar\omega \, \mathrm{Im}\left[(l_i+1)\left\{\sum_m \left[M^2_{l_i\, l}\frac{1}{2l+1}\tau^{00}_{lm\, lm}\right] + \widetilde{M2}_{l_i\, l}\right\}_{l=l_i+1} + l_i\{\ldots\}_{l=l_i-1}\right]$$

with radial matrix elements

$$M_{l_i\, l} = \int_0^{r_{MT}} dr\; r^3\, \phi^{core}_{l_i}(r)\, R^0_l(r)$$

and

$$\widetilde{M2}_{l_i\, l} = \iint dr\; r^3\, dr'\; r'^3\, \phi^{core}_{l_i}(r)\, R^0_l(r_<)\, S^0_l(r_>)\, \phi^{core}_{l_i}(r').$$

The important point to note is that the scattering path operator

$$\tau^{0\,0}_{lm\, lm} = \{[1 - T_a G_0]^{-1} T_a\}^{0\,0}_{lm\, lm}$$

can be expanded into successive terms representing scattering of the photoelectron off various centers. More formally, again we write (dropping the subscript on G from now on for convenience)

$$\tau = [1 - T_a G]^{-1} T_a = \sum_n (T_a G)^n T_a$$

where the last expansion is valid only where the spectral radius $\rho(T_a G)$ (maximum modulus of the eigenvalues) of the matrix $T_a G$ is less than unity.

Hence the total fine structure due to an excitation channel l is

$$\chi_l(\hbar\omega) = \frac{\sigma_l(\hbar\omega) - \sigma_l^0(\hbar\omega)}{\sigma_l^0(\hbar\omega)} = \frac{\sum_{n=2}^{\infty} \sigma_l^n(\hbar\omega)}{\sigma_l^0(\hbar\omega)}$$

where

$$\sigma_l^n(\hbar\omega) \cong \sigma_{l_i+1}^n(\hbar\omega) \cong \frac{8}{3}\pi^2\alpha\hbar\omega(l_i+1)\left\{\mathrm{Im}\left[\sum_m M_{l_i l}^2 \frac{1}{2l+1}\left[(T_a G)^n T_a\right]_{lm\,lm}^{00}\right]\right\}_{l=l_i+1}$$

and

$$\sigma_l^0(\hbar\omega) \cong \sigma_{l_i+1}^0(\hbar\omega) \cong \frac{8}{3}\pi^2\alpha\hbar\omega(l_i+1)\left\{\mathrm{Im}\left[\sum_m M_{l_i l}^2 t_l^0 - \tilde{M}2_{l_i l}\right]\right\}_{l=l_i+1}$$

In other words we have

$$\chi_l(\hbar\omega) = \frac{\sigma_l^2(\hbar\omega)}{\sigma_l^0(\hbar\omega)} + \frac{\sigma_l^3(\hbar\omega)}{\sigma_l^0(\hbar\omega)} + \frac{\sigma_l^4(\hbar\omega)}{\sigma_l^0(\hbar\omega)} + \cdots = \chi_l^2(\hbar\omega) + \chi_l^3(\hbar\omega) + \chi_l^4(\hbar\omega) + \cdots$$

using the plane wave limit for G and assuming real potentials

$$G^{ij}_{LL'} = -4\pi i\,(1-\delta_{ij}) \sum_{L''} i^{l-l'+l''} C^{L'}_{LL''} h^{+}_{l''}(\kappa R_{ij}) Y_{L''}(\hat{R}_{ij})$$

$$\approx 4\pi\, Y_L(\hat{R}_{ij})\, Y_{L'}(\hat{R}_{ij})\, \frac{e^{i\kappa R_{ij}}}{\kappa R_{ij}}$$

with

$\kappa \equiv \sqrt{E - V_{II}}$

and

$t^0_l(\kappa) \equiv e^{i\,\delta^0_l(\kappa)} \sin(\delta^0_l(\kappa))$

we obtain the form of the single scattering signal

$$\chi^l_2(\hbar\omega) = \frac{\sigma^2_l(\hbar\omega)}{\sigma^0_l(\hbar\omega)}$$

$$\cong \frac{\frac{8}{3}\pi^2 \alpha \hbar\omega\,(l_i+1)}{\sigma^0_l(\hbar\omega)} \left\{ \mathrm{Im}\left[\sum_m M^2_{l_i\, l} \frac{1}{2l+1} \left[T_a G T_a G T_a \right]^{00}_{l_m l_m} \right] \right\}_{l=l_i+1}$$

$$\cong \left\{ \frac{1}{\sin^2(\delta^0_l)} \frac{1}{2l+1} \mathrm{Im}\left[\sum_{\substack{m \\ l'm' \\ r}} t^0_l G^{0r}_{lm\, l'm'} t^r_{l'} G^{r0}_{l'm'\, lm} t^0_l \right] \right\}_{l=l_i+1}$$

$$\cong \mathrm{Im}\left\{ (-1)^l e^{i2\delta^0_l} \sum_r \frac{e^{i2\kappa R_{0r}}}{\kappa R^2_{0r}} \sum_{l'} \frac{t^r_{l'}\,(2l'+1)\,P_{l'}(\cos(\pi))}{\kappa} \right\}_{l=l_i+1}$$

$$\cong (-1)^{l_i+1} \sum_r \sin\{\, 2\delta^0_{l_i+1}(\kappa) + 2\kappa R_{0r} + \arg[f(\pi,\kappa)] \,\} \frac{\left| f(\pi,\kappa) \right|}{\kappa R^2_{0r}}$$

The third order signal is of the form

$$\mathrm{Im}\left[\sum_{\substack{r\ l'm' \\ s\ l''\ m''}}^{m} t^{0}_{l} G^{0r}_{lm}(l'm')\, t^{r}_{l'} G^{rs}_{l'm'}(l''m'')\, t^{s}_{l''} G^{s0}_{l''m''}(lm)\, t^{0}_{l} \right]$$

yielding a structure of the type

$$\sin\{\, 2\delta^{0}_{l_i+1}(\kappa) + \kappa[R_{0\,r} + R_{r\,s} + R_{s\,0}] + \arg[F(\kappa)] \,\} \; \frac{|F(\kappa)|}{\kappa R_{0\,r} R_{r\,s} R_{s\,0}}$$

and so on for higher order signals. The most general form of the n-th order signal is :

$$\chi_n^{l_i+1} = \sin\{\, 2\delta^{0}_{l_i+1}(\kappa) + \kappa P_{total} + \arg[F(\kappa)] \,\} \; \frac{|F^n(\kappa, R_{0\,r}, R_{r\,s}, R_{s\,t}, \ldots R_{v\,0})|}{\kappa\, R_{0\,r} R_{r\,s} R_{s\,t} \ldots R_{v\,0}}$$

In summary we note that:

1. Frequency goes like total path length

2. Amplitude decays with increasing path length

II. Application of XAS Method
A. Photodoping Effects in YBCO

Team Includes

J. F. Federici, NJIT

A. R. Bishop, Los Alamos Theory Group

A. Ignatov, NJIT

T. A. Tyson, NJIT

Observations

See A. Gilabert et al. J. Supercon. **13**, 1 (2000)

- Kudinov *et al.* Reported changes in the resistivity of $YBa_2Cu_3O_{6+x}$ with a maximum occurring near x=0.34 Phys. Rev. **47**, 9017 (1993).

- Unlike transient photoconductivity in YBCO with $\tau \sim 1$ ns

- Unlike photoconductivity in La_2CuO_4 with $\tau \sim 10$ s.

Photoconductivity exist for days if sample is kept at low temperatures

Two Models

1. Oxygen Ordering

Photodoping leads to ordering of oxygen atoms in the chains

2. Charge-Transfer

Photoabsorption creates electron hole pairs. The electron is trapped in chain defects while the holes contribute to the net number of carries

Phase diagram and photodoping model from Kudinov *et al.*

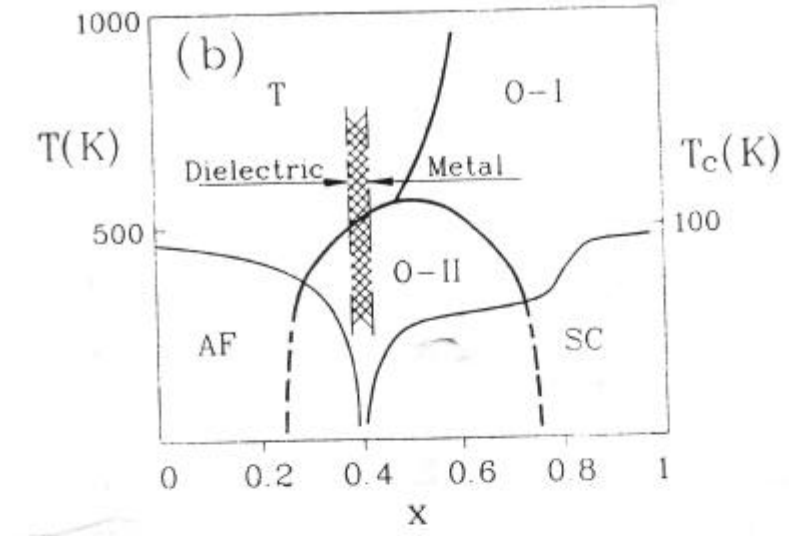

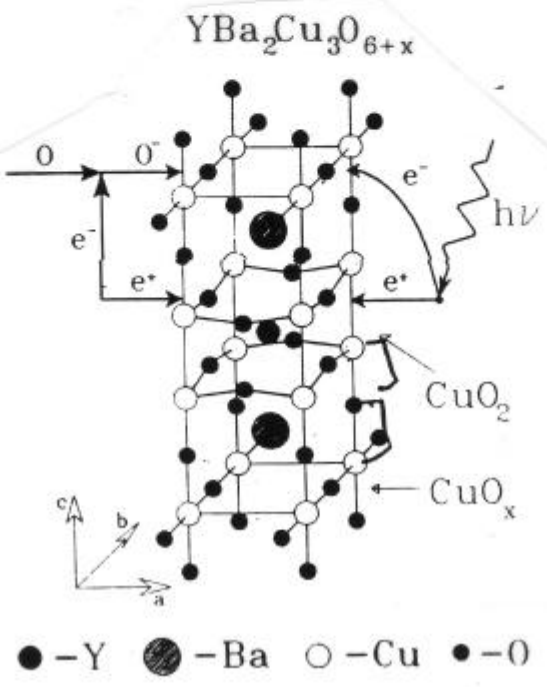

Unit Cell of YBCO (PRB 36, 5251 (1987))

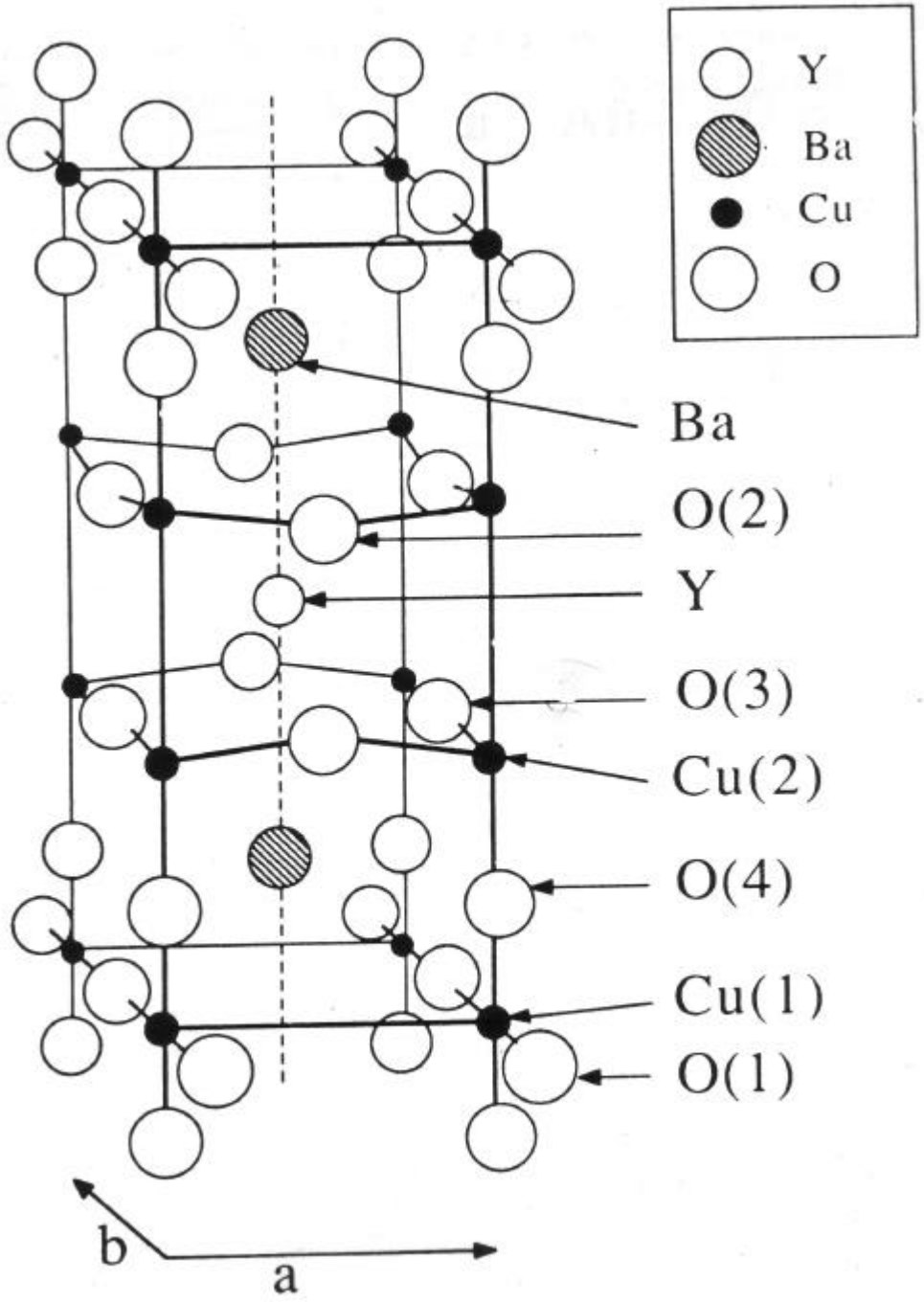

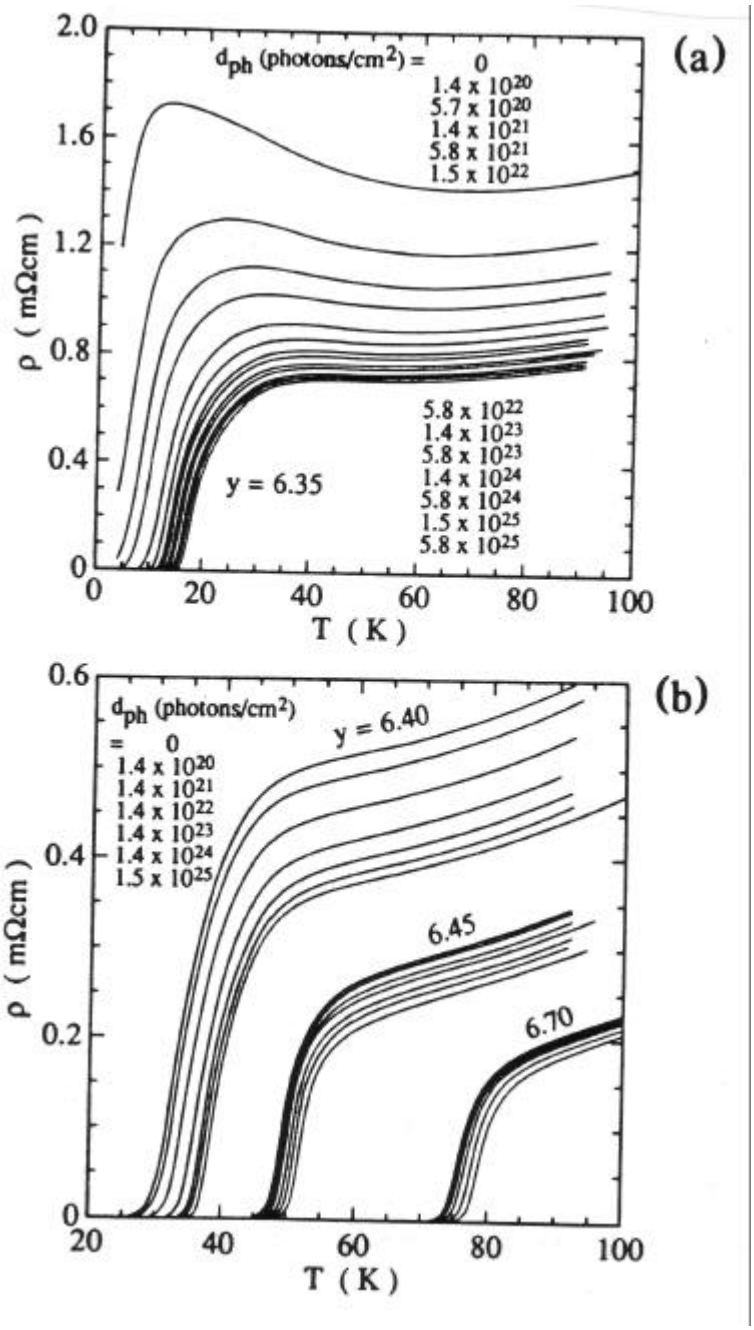

Effect of photodoping on the resistivity of YBCO as a function of oxygen content. Note that the largest effect is near x=0.35 (PRL 72, 1537 (1994))

Change in XRD pattern with photodoping. Note the contraction of the c-axis length.

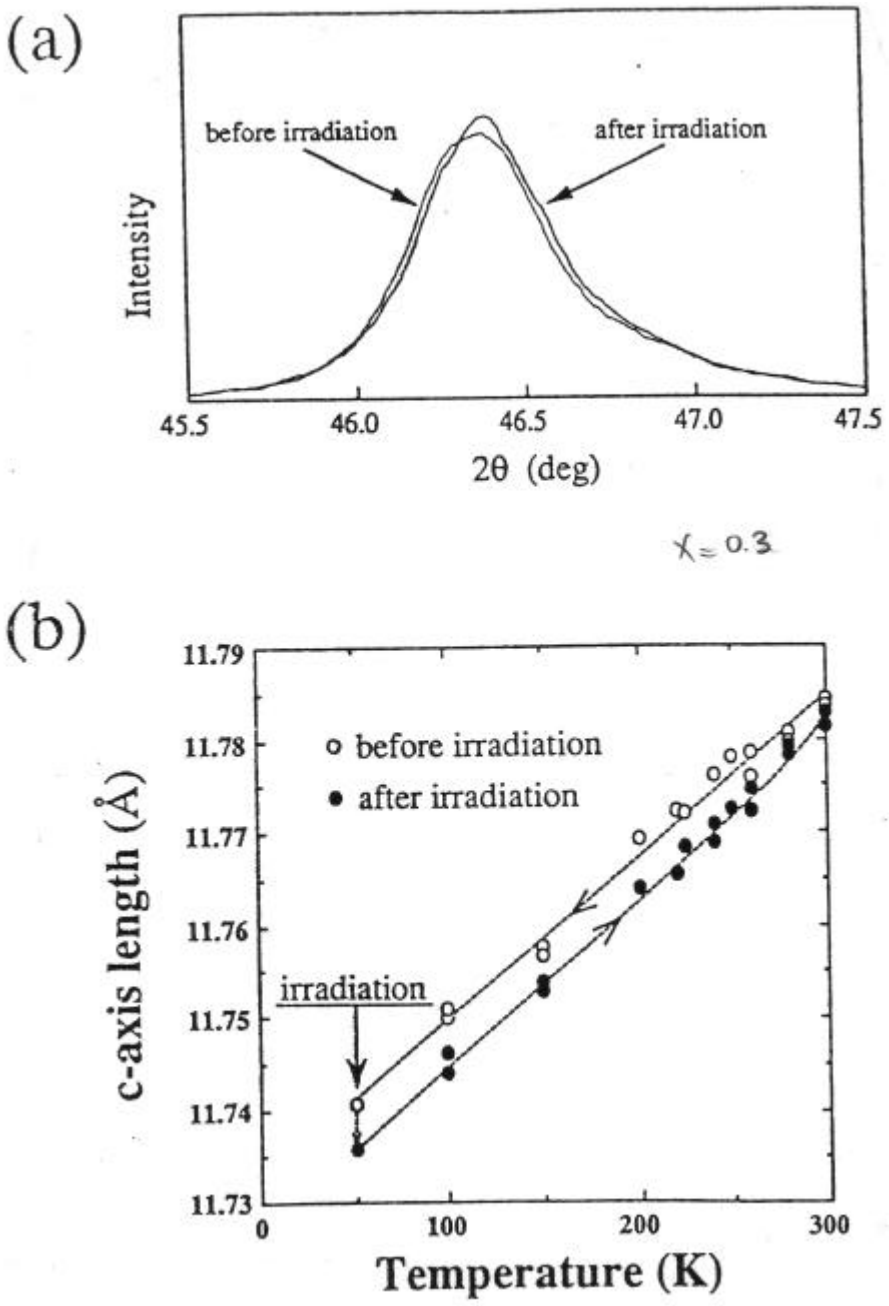

XRD reveals a narrowing of the 00L lines with photodoping

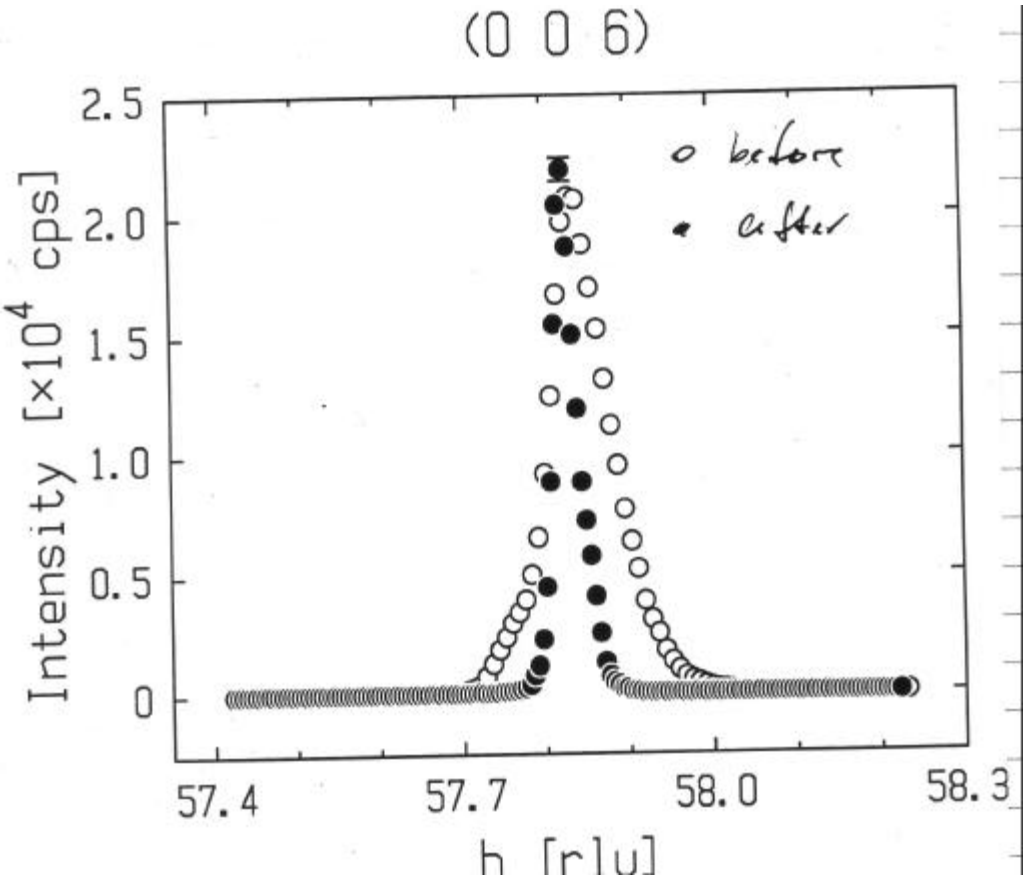

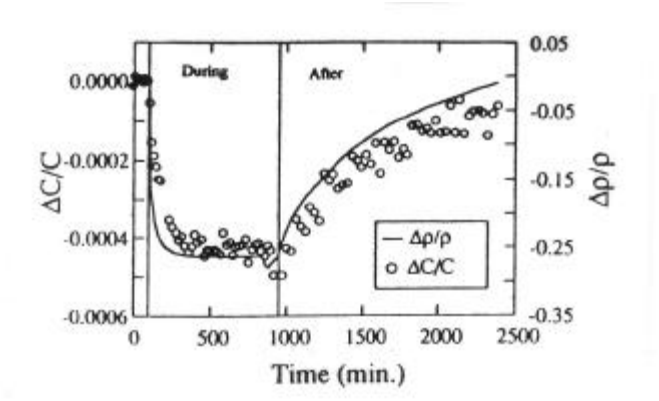

(a)

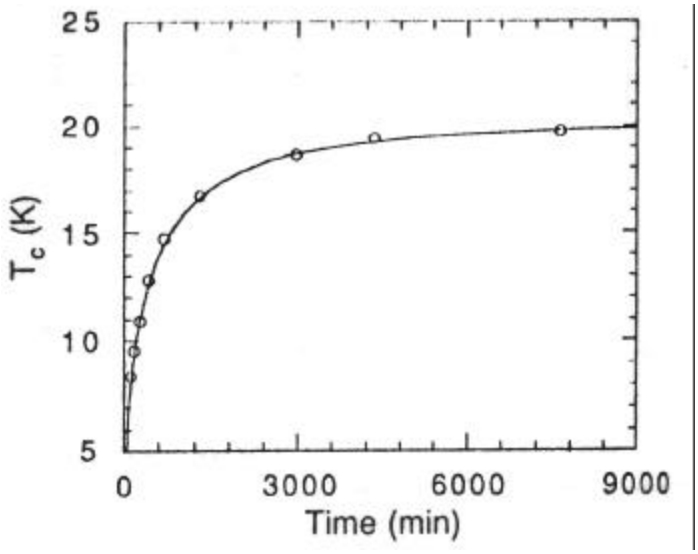

Comparison of the recovery of the resistivity and c lattice constant of photodoped YBCO (APL 64, 652 (1994) with the recovery of Tc in quenched YBCO powder (Physics C 167, 571 (1990)).

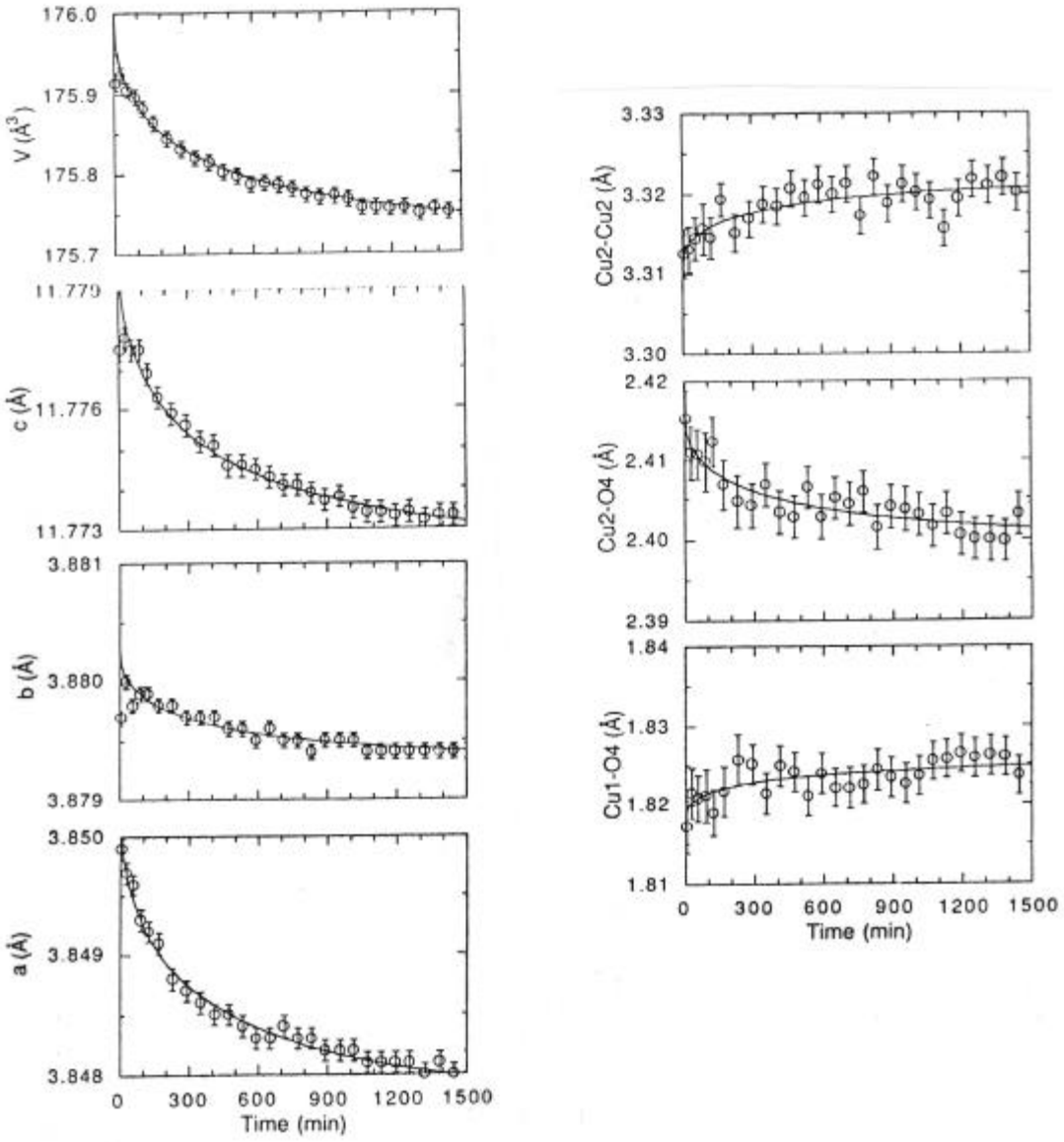

Recovery of lattice constants and bond distances in quenched YBCO powder (Physics C 167, 571 (1990)).

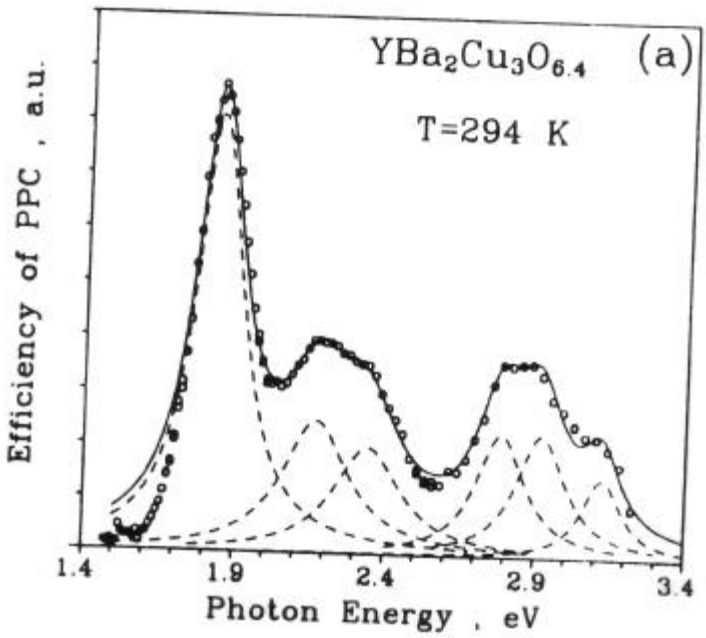

Photodoping efficiency as a function of photon energy measured at 294 K.

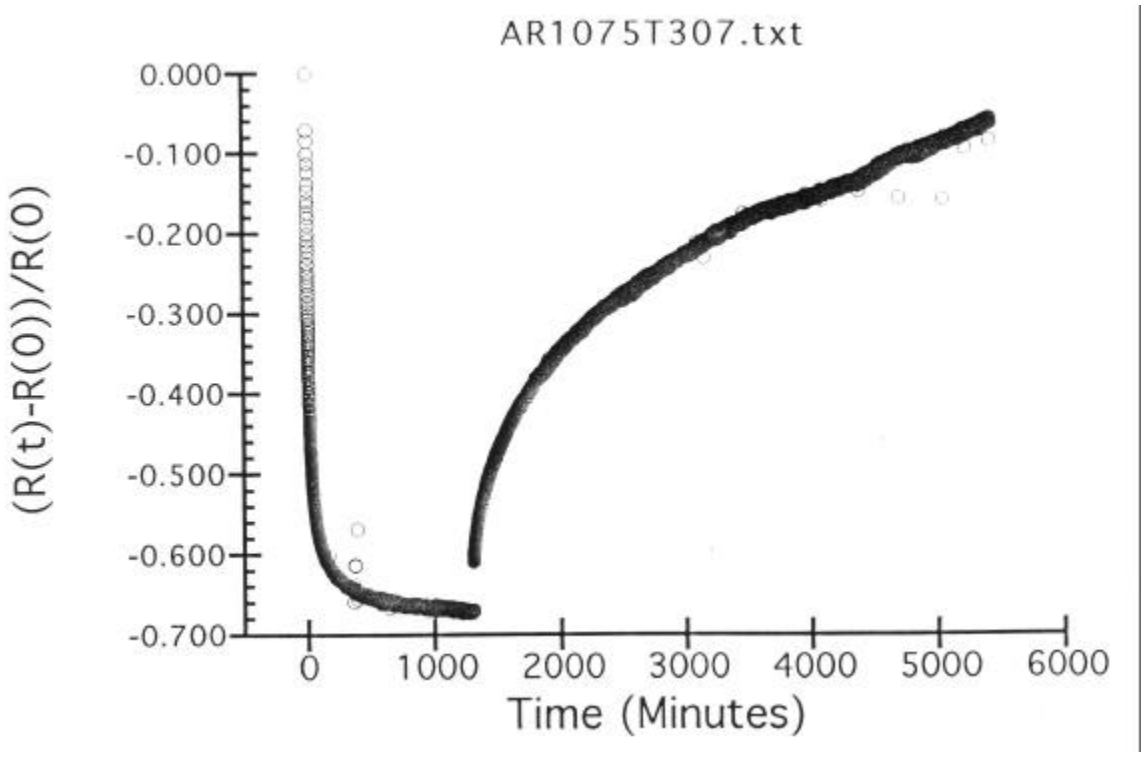

Measured response of film studies at 306 K.

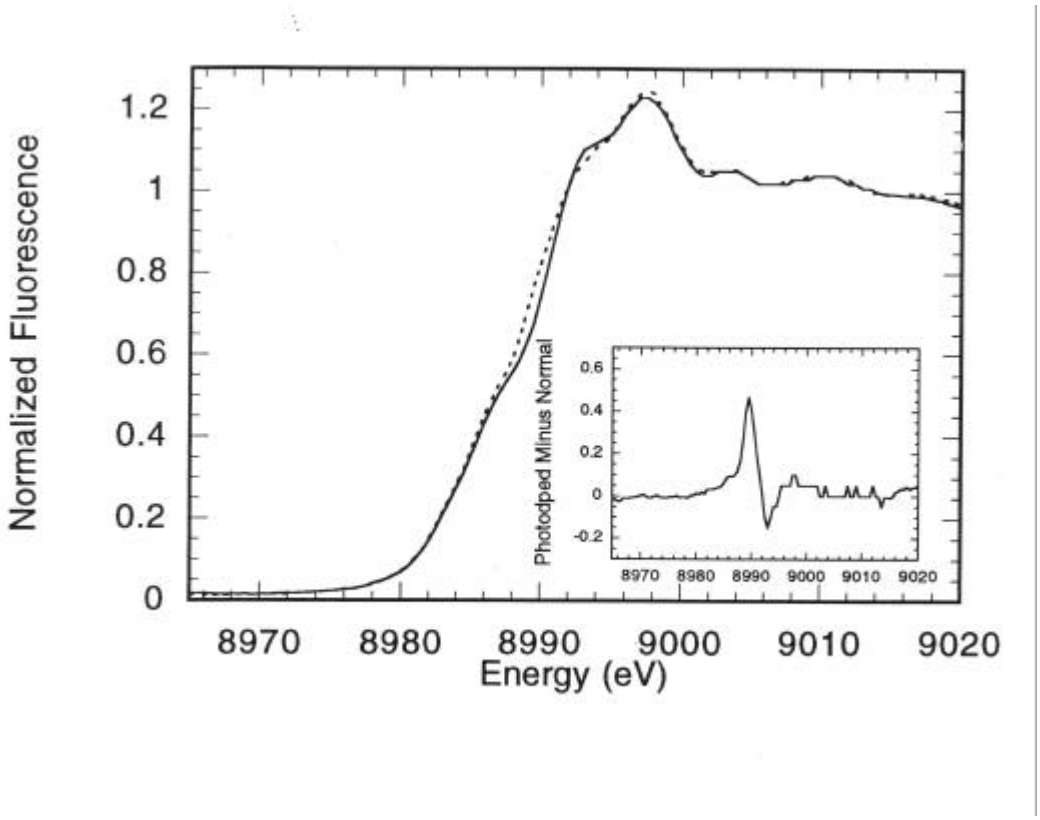

The XANES spectra of $YBa_2Cu_3O_{6.4}$ for the normal (solid line) and photodoped (dotted line) states reveal that photodoping induces a transfer of holes ($4p_z$) to Cu(2). The inset displays the difference between the two spectra. All measurements reported in this work were performed at 95 K. The quantitative structural information has been extracted from a detailed analysis of the high-energy EXAFS region.

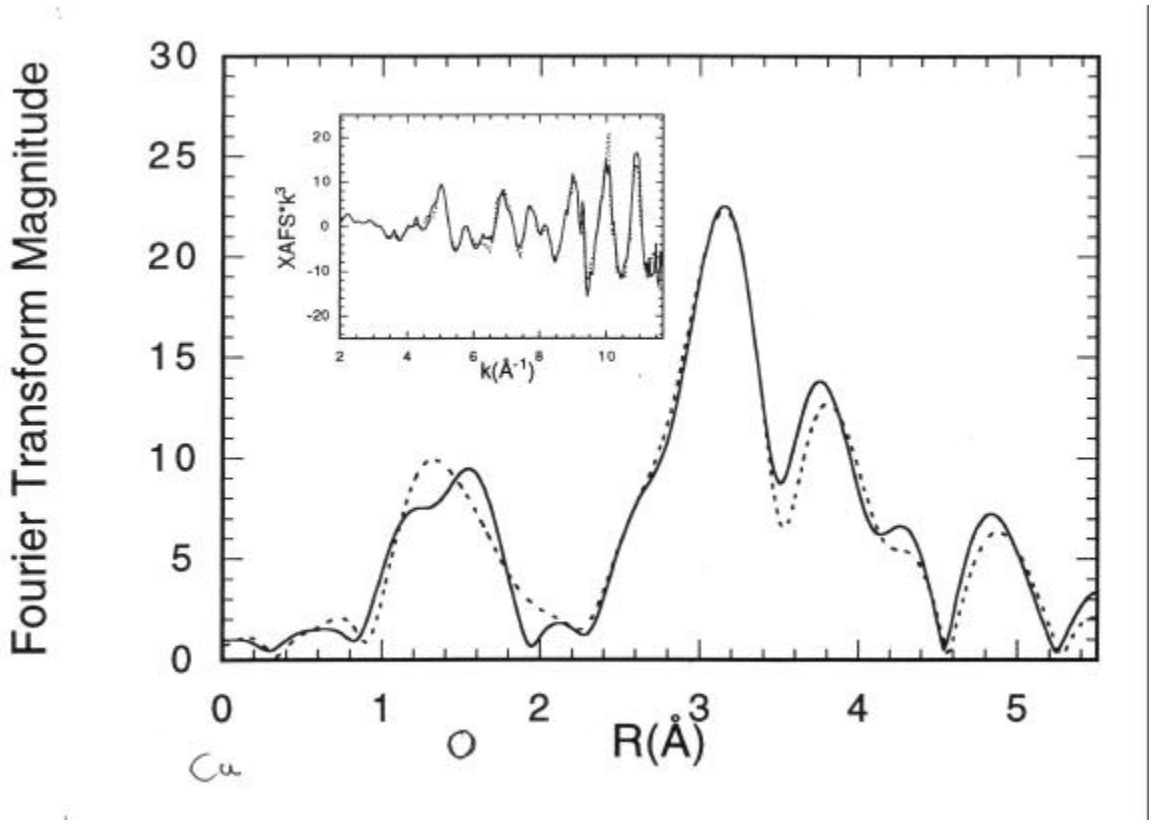

Magnitude of the Fourier transform of k^3∗XAFS for k = 2.8–11.7 Å^{-1} for normal (solid line) and photodoped (dotted line) $YBa_2Cu_3O_{6.4}$ system. The first peak (1-2 Å) corresponds to the c-axis Cu-O bond distribution. The second and third peaks centered near 3 Å and 4 Å contain the Cu(2)-Y/Cu(1,2)-Ba and Cu(2)-Cu(1) contributions, respectively. Changes occur both in the nearest neighbor Cu-O distribution and at the Cu(2)-Cu(1) position. Note that the peak positions in the raw Fourier transforms are at a shorter distance than the crystallographic bonds due to corrections from the central atom phase shift and the scattering atom phase function. The inset displays the corresponding raw data in k-space.

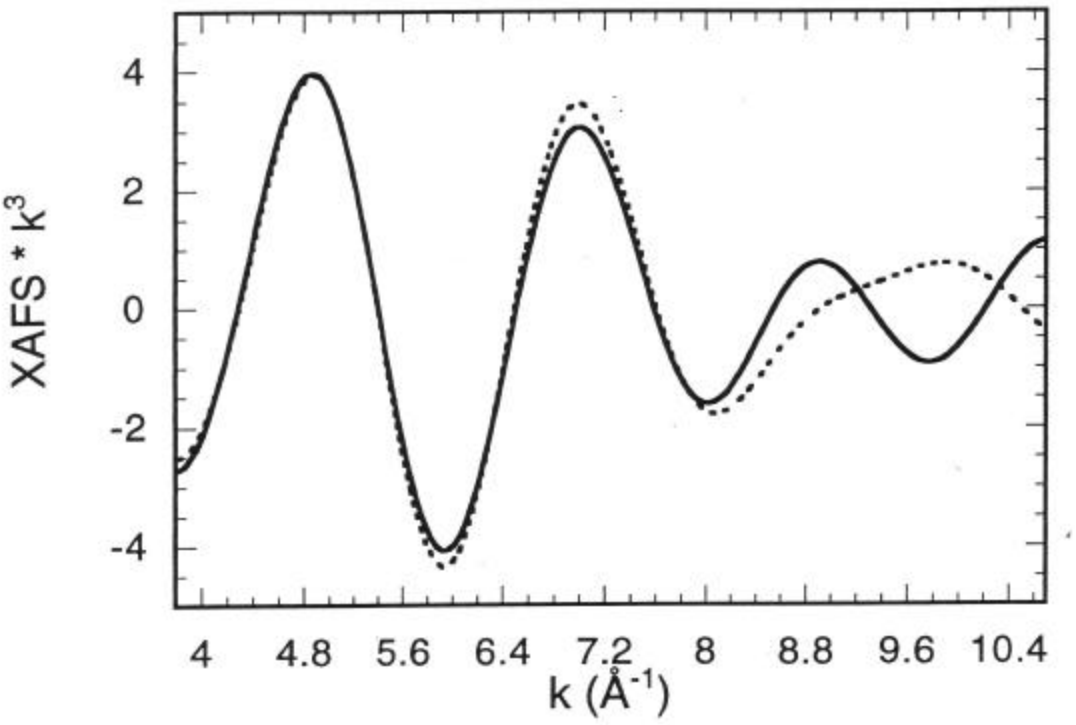

The Cu-O signals obtained by filtering the transformed data over the range 0.8-2.0 Å. The solid line and dotted lines correspond to the normal and doped systems, respectively. Note that a near cancellation of the doped signal occurs near $k \sim 9.6$ Å^{-1}. This "beat" is due to the interference of signals and indicates the presence of a pair of Cu-O peaks with close separation $\Delta r \sim \pi/2*k.=0.16$ Å

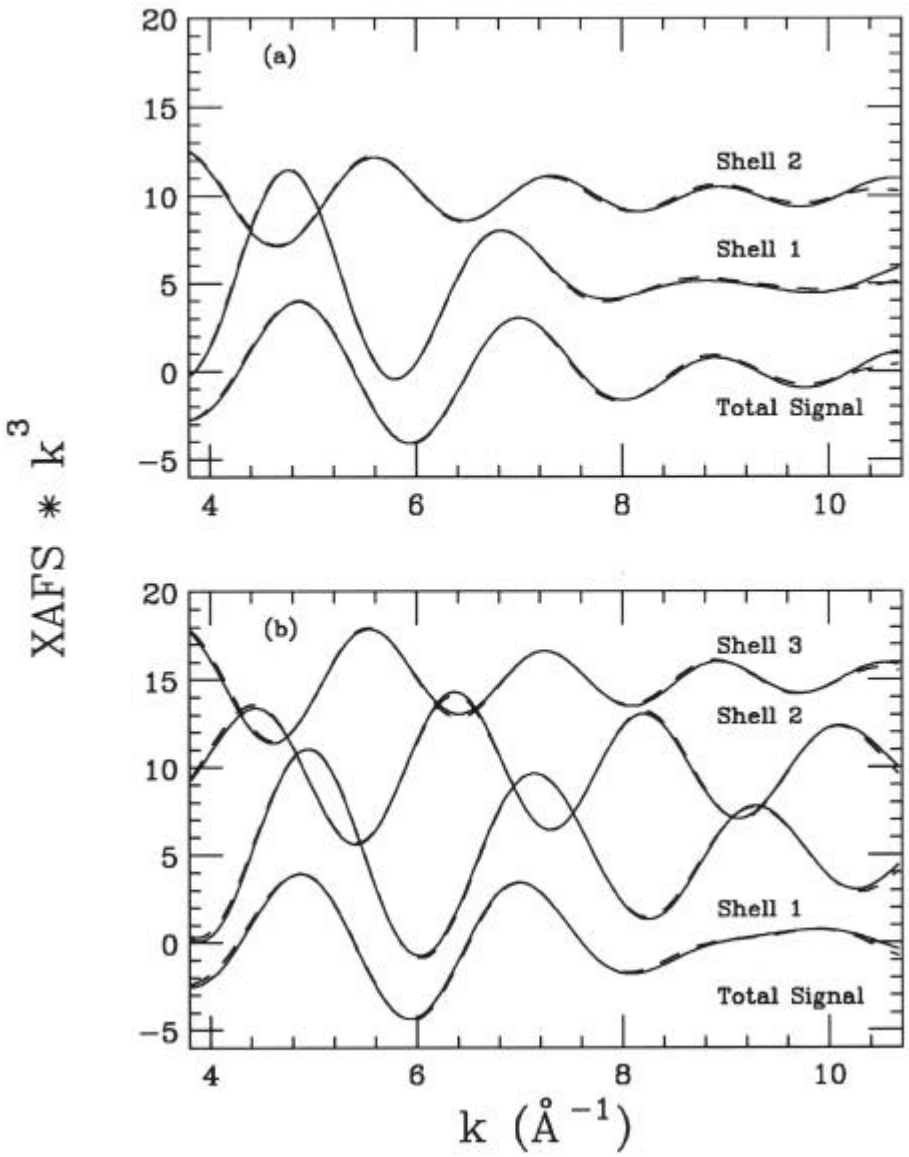

Model fit to the filtered signal for $YBa_2Cu_3O_{6.4}$ in the normal (a) and photodoped (b) states over the range 3.80 - 11.7 $Å^{-1}$. In panel (a), the total signal is given as the lower curve (solid line) with the full fit given by the dashed line. The individual components (shells) are also given with the theoretical model signal (see text) represented by the dashed lines. Shell 1 is at 1.87Å and shell 2 is at 2.25Å (Table I) . The solid line shown for each shell is the residual obtain by subtracting off all other shells from the total signal. In the case of the normal system only two c-axis Cu-O bonds (short Cu(1)-O(4) due to chains and long Cu(2)-O(4) due to planes) were found. Panel (b) displays the corresponding fits for the photodoped state with shell 1 is at 1.81 Å, shell 2 is at 2.00 Å and shell 3 is at 2.25Å.

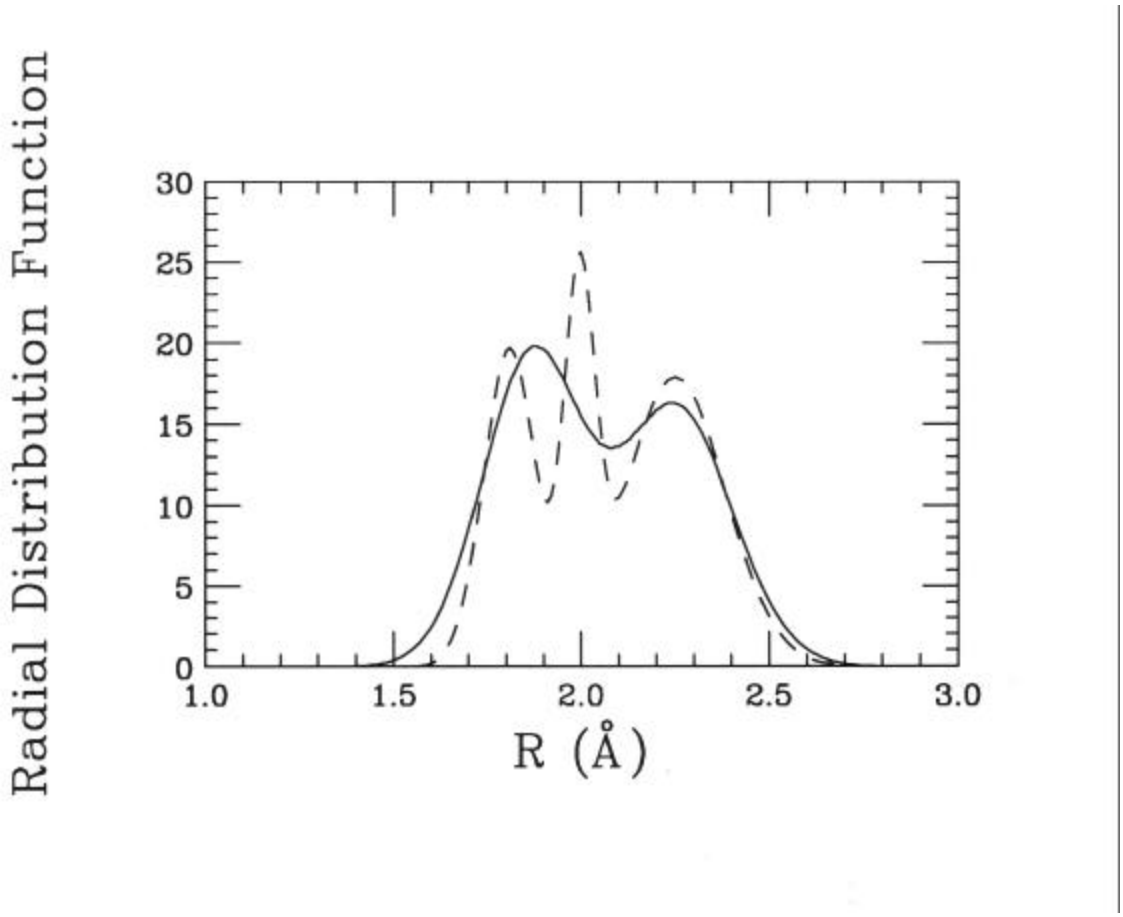

Generated radial distribution based on the Debye-Waller factors extracted from the Fit. The solid line corresponds to the undoped film and the dashed line corresponds to the doped sample. Note the sharpening of the short Cu-O bonds due to photodoping.

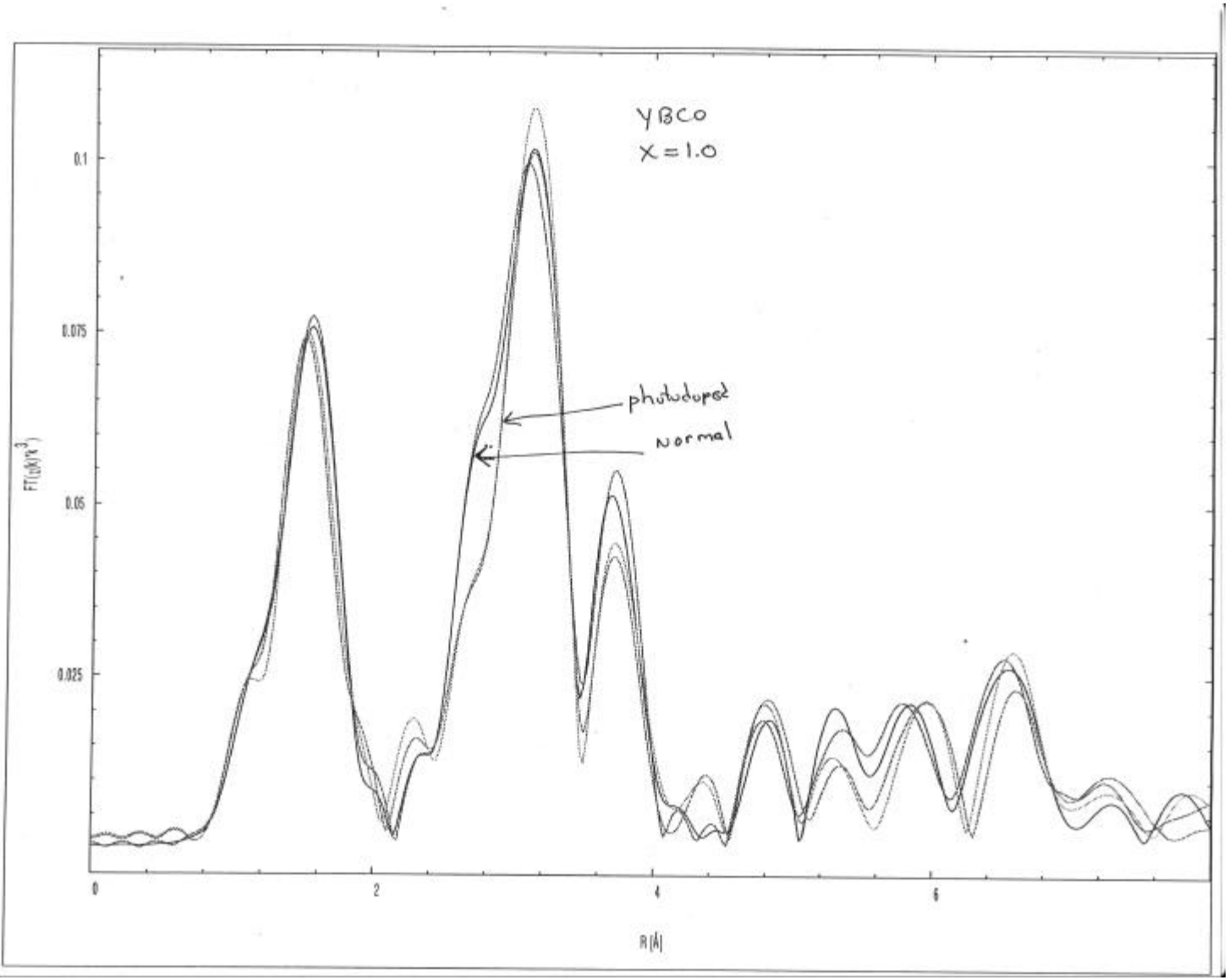
YBCO
X=1.0
photodoped
normal
0.1
0.075
0.05
0.025
FT(ΔA/R^3)
0
2
4
6
R(Å)

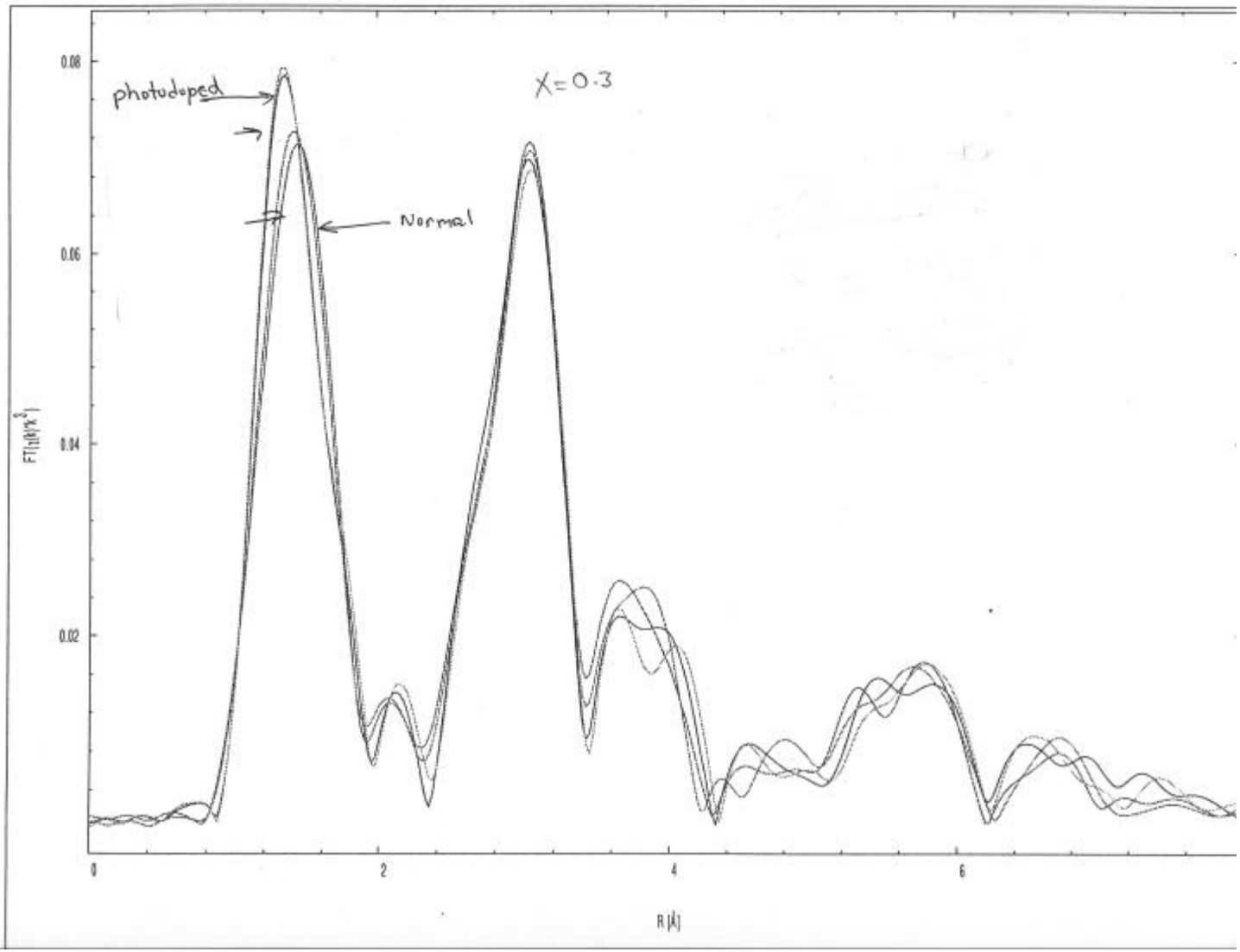
photodoped
X=0.3
Normal
0.08
0.06
0.04
0.02
FT[Q(R)/X^3]
0
2
4
6
R[Å]

Summary of Main Results

Evidence of hole transfer into the CuO_2 planes accompanying photodoping is found

A local distortion of the CuO_x chains is observed

The results are consistent with photoinduced chain ordering.